When size matters: differences in demineralized bone matrix particles affect collagen structure, mesenchymal stem cell behavior, and osteogenic potential

Title

When size matters: differences in demineralized bone matrix particles affect collagen structure, mesenchymal stem cell behaviour, and osteogenic potential.

Short title

DBM particle size affects collagen structure

Authors

Dozza B[1,2*], Lesci IG[3], Duchi S[1], Della Bella E[4,5], Martini L[4], Salamanna F[4],Falconi M[6], Cinotti S[7] , Fini M[4], Lucarelli E[1] and Donati D[1,2]

[1]Osteoarticolar Regeneration Laboratory, 3rd Orthopaedic and Traumatologic Clinic prevalently Oncologic, Rizzoli Orthopaedic Institute, via di Barbiano 1/10,40136 Bologna, Italy

[2]Department of Biomedical and Neuromotor Sciences (DIBINEM), Alma Mater Studiorum University of Bologna, via G. C. Pupilli 1, 40136 Bologna, Italy

[3]WAPH Technology Corp. 1920 N Commerce Parkway, Weston, FL 33326, US

[4]Laboratory of Preclinical and Surgical Studies, Rizzoli Orthopaedic Institute, via di Barbiano 1/10,40136 Bologna, Italy

[5]Department of Experimental, Diagnostic and Specialty Medicine (DIMES), Alma Mater Studiorum University of Bologna, via G. Massarenti 9, 40138 Bologna, Italy

[6]Department of Biomedical and Neuromotor Sciences (DIBINEM), division of Human Anatomy, Alma Mater Studiorum University of Bologna, via Irnerio 48, 40126 Bologna, Italy

[7]Cell Culture Centre, Istituto Zooprofilattico Sperimentale della Lombardia e dell'Emilia Romagna (IZSLER), via Bianchi 9, 25124 Brescia, Italy

*Corresponding author
Dr. Barbara Dozza
Osteoarticular Regeneration Laboratory; 4th floor, Scala B, Rizzoli Orthopaedic Institute, via di Barbiano 1/10, 40136 Bologna (BO), Italy
Phone: +39-051-6366595
Fax: +39-051-6366799
E-mail: barbara.dozza@ior.it

Abstract

Demineralized bone matrix (DBM) is a natural, collagen-based, osteoinductive biomaterial. Nevertheless, there are conflicting reports on the efficacy of this product. The purpose of this study was to evaluate whether DBM collagen structure is affected by particle size and can influence DBM cytocompatibility and osteoinductivity. Sheep cortical bone was ground and particles were divided in three fractions with different sizes, defined as large (L, 1- mm), medium (M, 0.5-1 mm), and small (S, < 0.5 mm). After demineralization, the chemical-physical analysis clearly showed a particle size-dependent alteration in collagen structure, with DBM-M being altered but not as much as DBM-S. DBM-M displayed a preferable trend in almost all biological characteristics tested, although all DBM particles revealed an optimal cytocompatibility. Subcutaneous implantation of DBM particles into immunocompromised mice resulted in bone induction only for DBM-M. When sheep MSC were seeded onto particles before implantation, all DBM particles were able to induce new bone formation with the best incidence for DBM-M and DBM-S. In conclusion, the collagen alteration in DBM-M is likely the best condition to promote bone induction *in vivo*. Furthermore, the choice of 0.5-1 mm particles may enable to obtain more efficient and consistent results among different research groups in bone tissue-engineering applications.

Keywords

Demineralized bone matrix; particle size; collagen structure; osteoinduction; mesenchymal stem cells.

INTRODUCTION

Suitable bone grafts are needed in the fields of orthopaedics, neurosurgery, dentistry, and cranio-maxillofacial surgery to stimulate bone healing.[1] The autologous graft is the gold standard in bone reconstruction procedures, because it accomplishes osteoconduction, osteoinduction and osteogenesis.[2] However, the use of autologous grafts is limited by both the finite supply and the potential post-operative complications associated with their procurement. Furthermore, the harvested bone has a precise size and shape and a critical step is to adapt it to the defect that needs

to be treated. Therefore, there is a great demand for bone substitutes that are not limited, can fit the defect that needs to be treated, and are readily available.

Nowadays several bone substitutes are available on the market and according to their origin they are mainly divided into two categories: natural and synthetic substitutes.[3–6] Both of them display osteoconductive and/or osteoinductive properties, but commonly they lack osteogenic potential due to the absence of viable osteoprogenitor cells.[7] Among the natural bone substitutes, demineralized bone matrix (DBM) has been extensively used for clinical repair of skeletal defects and bone abnormalities, including non-union fractures, bone cysts, cranio-maxillofacial reconstructions, and periodontal diseases.[8] DBM is prepared by pulverization of native osseous tissue, followed by acid extraction of the mineral phase of bone which results in a variable percentage of residual calcium phosphate. This process, largely developed by Urist in 1965, results in a composite of matrix proteins, mainly collagen, and growth factors, including bone morphogenetic proteins (BMPs).[9] The demineralization process exposes collagen fibers and osteoinductive factors normally contained in the bone tissue, making them more bio-available. Therefore, DBM could potentially be more osteoinductive than standard mineralized allograft.[10,11] So far, the use of DBM in orthopaedic and periodontal applications has been reported, notwithstanding a variability in the efficacy in the results presented. Several studies indicate that different factors such as donor age, gender, method of preparation, particle size and conditions of storage and of sterilization can affect DBM's osteoinductive property. [8,12–15] Therefore, in order to have more coherent clinical results, a more consistent DBM product should be developed. This requires pooling DBM obtained from a pool of donors, and paying specific attention to the critical phases of the production to ensure the desired product features. As far as we know only three studies regarding the influence of DBM particle size on the induction of new bone formation have been published and have provided important indications. Syftestad and Urist [16] performed experiments in rats and showed that the incidence of new bone induced by implants of demineralized whole matrix powders of 125- 50 μm and 500-1000 μm approached 100%, while bone yield was almost completely absent in demineralized whole

matrix pulverized to 44-75 μm. Sampath and Reddi [17] also demonstrated that DBM particle size is a critical factor in triggering the biochemical cascade of endochondral bone differentiation. Subcutaneous implantation of 74-4 0 μm DBM particles into allogeneic rats resulted in the local differentiation of bone, whereas implantation of 44-74 μm particles did not. Zhang and colleagues [12] showed that DBM particles ranging from 500 to 710 μm provided the highest level of calcium deposition after implantation in muscle pouches of athymic mice, whereas particles less than 250 μm showed the lowest level of calcium deposition. In complex these studies demonstrate that the particle size is important: smaller DBM particles are less effective than larger DBM particles, even if the reason behind these results has not yet been elucidated.

Given that collagen is the major component of DBM, in this study we evaluated whether collagen structure is affected by particle size. The influence of collagen alteration and particle size on the cytocompatiblity and osteoinductive potential of DBM was also investigated *in vitro* and *in vivo*.

MATERIALS AND METHODS

Preparation of DBM

Cortical bone was harvested from the femurs and tibias of ten sheep. Soft tissues were removed and the bones were cut into circular segments of diameters less than 1 cm long. The bone segments were then rinsed in distilled water to remove any remaining marrow and blood within the bone and stored at -80°C until the demineralization protocol was performed. Demineralized bone matrix (DBM) powder of three different particle size was prepared according to the protocol by Reddi and Huggins [18] with some modification. Frozen bone segments were first ground into particles of a size less than 2 mm using a centrifugal mill (ZM100, Retsch GmbH, Haan, Germany). The rotor of the centrifugal mill was first refrigerated to reduce the temperature to which the bone particles were exposed during pulverization. Then three different particles size fractions were obtained by stratification with a nested column of sieves. Each sieve in the column had a wire mesh cloth with openings smaller than the sieve above. We obtained the following fractions with particles of

discrete size ranges. Fraction 1: large particle size (L), 1 mm- mm; fraction 2: medium particle size (M), 0.5 mm-1 mm; fraction 3: small particle size (S), < 0.5 mm. Each fraction was rinsed in absolute ethanol and in diethyl ether for 1 h each, with one change of each solution. Particles were then demineralized in 1N HCl for 80 min, changing the solution three times. After demineralization, the HCl was decanted and the DBM particles were washed three times in distilled water for a total period of 1 h. Each sample was then rinsed in absolute ethanol and in diethyl ether for 20 min each and then dried at room temperature under a laminar flow hood overnight. Each DBM sample was lyophilized in a vacuum chamber (0,0052 mbar) at −48°C (Labconco, FreeZone 2.5 Liter Benchtop Freeze Dry System) for 48 h. Packaged DBM particles were then sterilized by irradiating them with 25 KGy of gamma radiation. The particles were then categorized as DBM-Large (DBM-L), DBM-Medium (DBM-M), or DBM-Small (DBM-S) according to particle size of fraction 1, 2, and 3 respectively. Radiographs of each fraction were carried out to assess the demineralization process.

Chemical-physical characterization of DBM samples

Inductively coupled plasma optical emission spectroscopy

The calcium content in the bone particles before demineralization and in DBM samples has been measured with inductively coupled plasma optical emission spectroscopy (ICP-OES) using a ICP MOD. JY ULTIMA2 to allow the rapid determination of 15 elements in the wavelength range of 160-800 nm. ICP-OES analysis has been carried out on sample solutions prepared according to an acidic dissolution (nitric acid) of the samples inside hermetically sealed Teflon holders processed in a microwave mineralizer Milestone Model MLS 1200. The calcium determination was performed in triplicate and results were plotted as mean values ± SD. Data obtained from demineralized samples were compared by a two-tailed t test. Differences were considered statistically significant for a $p < 0.05$.

Fourier Transform infrared spectroscopy

The infrared spectra were measured from 4000 to 400 cm^{-1} with 4 cm^{-1} resolution using a Nicolet 380 spectrometer. Other settings include an 8 mm aperture, 128 scans, velocity of 10 kHz,

DLATGS detector, and a 3-term Blackman-Harris apodization function. KBr pellets were obtained under vacuum, using 1 mg of the powdered samples carefully mixed with 200 mg of infrared grade KBr.

X-Ray Diffraction

Structural characterization was performed for DBM characterization with X-Ray Diffraction (XRD) analysis. Data were collected using a PANalytical θ/θ diffractometer (CuKα radiation; 40 kV and 40 mA) equipped with a real-time multiple strip (RTMS) detector. Data were collected in the continuous mode, with Ni filtration of the primary beam, the divergence slits fixed at 1/41, 0.00231 Soller slits on the incident and secondary beams, a fixed 1/41 antiscatter slit, and a fixed 5-mm RTMS slit. The integrated step scan mode of the RTMS detector (0.01671 2θ) was used, with 50 s/step.

Differential Thermal Analysis

Differential Thermal Analysis (DTA) was performed using a Q600 TA Instruments. About 5 mg of DBM powder for each size was used in each measurement and the heating rates used were 10 °C min^{-1}. The DTA measurements were conducted in an open alumina-pan and in a nitrogen atmosphere with a flow rate of 100 mL min^{-1}. The investigated temperature ranges were: 25-1000 °C for all samples. The TGA (Thermal Gravimetric Analysis) apparatus was calibrated in terms of mass and temperature. Calcium oxalate was used for the sample mass calibration. The melting points of three compounds (indium, aluminum, and copper) obtained from the DTA signals were used for the sample temperature calibration. The temperature accuracy of the TGA/DTA system is about ± 0.25 °C. The weighting accuracy is around 0.1 mg, which corresponds to 0.001% for a 10 mg sample.

Isolation and cultivation of bone marrow-derived mesenchymal stem cells

Primary bone marrow–derived mesenchymal stem cells (MSC) were isolated from the iliac marrow of adult sheep as previously reported. [19] Briefly, the nucleated cells were isolated by a density

gradient solution (Ficoll-Paque PREMIUM, Ge Healthcare, Uppsala, Sweden) and selected by plastic adherence. Cells of passage 3-4 were used for the study.

Cell seeding and cell seeded-DBM culturing

MSC seeded-DBM was produced by a two-step seeding procedure. Aliquots of 0.1 cc of each DBM fraction were placed in 1.5 mL tubes that function as seeding vessels, rehydrated with Dulbecco's phosphate-buffered saline (D-PBS, Euroclone, Milan, Italy), and submerged in culture medium overnight at 37 °C. The day after, the medium was removed and the DBM particles were drop-seeded with 100 μL of a concentrated cell suspension containing four different total cell numbers: 2×10^5, 4×10^5, 8×10^5, and 1.6×10^6. The seeding vessels were placed on a rocker (Vari-Mix rocker, ThermoLyne, Thermo Fisher Sci., Inc) oscillating at 10 rpm and incubated for 2 h in a humidified incubator (37°C, 5% CO_2 and a relative humidity of 95%) to allow for initial cell attachment. One ml of fresh cell culture medium was then slowly added to each vessel and statically cultured for additional 18 h. The following day (day 1) the residual seeding medium was removed, the MSC-seeded DBM particles were gently rinsed with 600 μl D-PBS, and were analyzed (see details below) or cultured under static culture conditions for another 48 h (day 3). Cell-free particles were incubated under similar conditions and served as controls.

DBM cytocompatibility

Cell Seeding Efficiency

Cell seeding efficiency (CSE) was performed using an indirect method. The CSE was calculated based on the number of unattached cells that ended up in the residual seeding medium using the following equation:

$$CSE = 1 - \frac{cells_u}{cells_i} \times 100\ \%$$, where $cells_i$ is the number of cells initially seeded and $cells_u$ is the number of unattached cells in the residual seeding medium and in D-PBS used for rinsing cell-seeded DBM at day 1. Unattached cells were counted by a hemocytometer (trypan blue assay) and an automatic cell counter (NucleoCounter, ChemoMetec A/S, AllerØd, Denmark). Two

independent samples of cells from three different MSC donors were evaluated and results were expressed as mean ± standard deviation. Statistical analysis was performed by two-way analysis of variance (ANOVA). Bonferroni's test for multiple comparisons was used as post-hoc comparison between different groups. The statistical program GraphPad-Prism5 (GraphPad Software, San Diego, CA, USA) was used for the analysis.

Metabolic cell activity

The overall metabolic cell activity of the MSC-seeded DBM samples was monitored at day 1 and day 3 of culture using the nontoxic Alamar Blue assay according to the manufacturer's instructions.[20] Before measurements the constructs were transferred into new wells to avoid the influence of potential unattached cells. Non-seeded DBM samples were likewise analysed as blank controls to adjust for background fluorescence. Two independent samples of cells from three different MSC donors were evaluated and results were expressed as mean ± standard deviation. Statistical analysis was performed as described in the previous section. After measurement of overall metabolic cell activity, the constructs were analyzed to evaluate cell viability and distribution.[21,22]

High resolution scanning electron microscopy

MSC were cultured on DBM particles for 1 and 3 days and then were processed for high resolution scanning electron microscopy (HR-SEM) analysis to evaluate cell morphology. The samples were fixed with a solution of 2.5% glutaraldehyde in 0.1 M phosphate buffer (Sigma Aldrich, St. Louis, Missouri, USA) for 2 h at 4 °C and subsequently with 1% OsO_4 for 1 h at room temperature (RT). The samples were dehydrated in an ascending alcohol series and critical point dried (CPD 030, Bal-tec, Leica Microsystems GmbH, Wetzlar, Germany). The samples were then metal-coated with a thin layer of carbon/platinum (030, Bal-tec, Leica Microsystems GmbH, Wetzlar, Germany) and observed under HR-SEM (JSM 890, Jeol Company, Tokio, Japan) with 7 kV accelerate voltage and $1x10^{-11}$ mA.

Cell viability and distribution

MSC seeded-DBM samples were assessed for viability and distribution with LIVE/DEAD® viability/Cytotoxicity Kit (L-3 4; Molecular Probes, Eugene, OR, USA) according to the manufacturer's instructions. Green-fluorescent calcein-AM was used to detect intracellular esterase activity, while red-fluorescent EthD-1 was applied to stain dead cells. Samples were observed with a fluorescent microscope (Nikon Eclipse TE2000-U, Nikon, Tokio, Japan) equipped with a Nikon DS-Vi1-U3 CCD digital camera. Furthermore, imaging was performed with a Nikon Eclipse Ti inverted microscope equipped with an A1R confocal laser scanner (Nikon, Netherland) and temperature-CO controllers (Okolab, Ottaviano, Naples, Italy). *z*-stacks images were acquired with Nikon Plan Apo VC 20x/0.75NA DIC N2 objective lens every 2 μm and 3D rendering was performed with NIS elements software using the *Alpha-blending* algorithm.

DBM osteoinductivity

In vitro bioassay

The *in vitro* bioassay to test DBM osteoinductivity was conducted as previously described by Maddox and colleagues.[23] Briefly, MSC were plated onto six-well tissue culture plates in αMEM containing 10% FBS. The cells were grown to 70% of confluence (day 0) and the media was changed to αMEM containing 2% FBS (control, CRL), or 2% FBS plus a specific DBM fraction (DBM assay medium) to evaluate its osteogenic potency. Approximately 0.1 cc of DBM powder from the three different size fractions was added to the appropriate well. The culture medium was renewed every 3-4 days.

Gene expression of selected markers was analyzed by quantitative reverse transcription polymerase chain reaction (qRT-PCR). Total RNA from cultured MSC (day 2 and day 6 of culture) was isolated using a phenol-chloroform extraction with TRIzol reagent (Invitrogen, Carlsbad, CA, USA) and checked for integrity by gel electrophoresis and spectrophotometrically quantified with NanoDrop 2000 (Thermo Scientific, Waltham, MA, USA). cDNA was prepared using the Superscript Vilo cDNA synthesis kit (Life Technologies), following the manufacturers' instructions. The cDNA was

amplified in duplicate by QuantiTect SYBR green PCR kit (Qiagen, Hilden, Germany) in a Light Cycler 2.0 Instrument (Roche Diagnostics GmbH, Manheim, Germany), using specific primers for sheep genes (Integrated DNA Technologies, IDT, Coralville, IA, USA) (Supporting information, Table S1). The gene expression of selected markers was normalized to the housekeeping gene glyceraldehyde-3-phosphate dehydrogenase (*GAPDH*) and the relative expression of target genes was determined using the $2^{-\Delta\Delta Ct}$ method, [24] using the CRL sample at day 2 as calibrator.

At days 6 and 13 of culture with or without DBM fractions, MSC were examined by light microscopy and photographed after Alizarin red S staining to detect the presence of calcium deposition by cells of an osteogenic lineage.[25] Microscopic images of osteogenic differentiation were acquired with an inverted Nikon Eclipse TE2000-U microscope (Nikon, Amsterdam, Netherlands), equipped with a Nikon DS-Vi1-U3 CCD color digital camera and a Nikon Plan Fluor 4×/0.13NA objective lens.

In vivo bioassay

Comparison of *in vivo* osteoinductivity between different particle size DBM samples was carried out by subcutaneous ectopic bone formation assay. The osteoinductive potential of DBM was also assessed by cultivating MSC on different DBM particles 1 day before implantation in order to evaluate whether particle size affects MSC potential contribution to osteoinductivity.

The experimental protocol was approved by the Ethical Committee of Rizzoli Orthopaedic Institute and by the Italian Ministry of Health. Thirty immune-compromised NU/NU male mice (5-6 week-old) (Harlan Laboratories Srl, Udine, Italy) were used in this study. Non-seeded or MSC-seeded DBM particles of each fraction (DBM-L, DBM-M, DBM-S) were subcutaneously implanted into left or right side pockets formed in the dorsal surface of the mice. Two implants were made on each mouse. Experimental groups included: (1) DBM-L; (2) MSC-seeded DBM-L; (3) DBM-M; (4) MSC-seeded DBM-M; (5) DBM-S; (6) MSC-seeded DBM-S. Each group consisted of ten implants. DBM particles (0.4 cc) were inserted on the left pocket and the corresponding MSC-seeded DBM particles on the right pocket. Sheep MSC derived from one donor at P3 (3.2×10^6 cells) were seeded

onto DBM particles 1 day before implantation. After 8 weeks, the animals were euthanized and the implants were retrieved for *ex-vivo* analyses. Ten implants were retrieved for each group, of which five were used for histology and five for gene expression analyses.

For histological examination five retrieved implants were fixed in 10% buffered formalin for about 24h, washed in distilled water, superficially decalcified in a 5% nitric/formic acid solution, dehydrated in a graded series of alcohols and, finally, embedded in paraffin. Five-micrometer-thick sections were obtained by a Microm HM340E (Microm International GmbH, Heidelberg, Germany) and stained with haematoxilin and eosin (H&E), Masson trichrome or toluidine blu/fast green. Ten microscopic fields per section were randomly observed with an optic microscope (Olympus-BX51, Germany) connected to an image analyzer system (Leica-Qwin, UK). The same implants were also stained for tartrate-resistant acid phosphatase (TRAP), a marker enzyme specific for osteoclasts.[26] Briefly, sections were deparaffinised and TRAP staining was performed using a commercial acid phosphatase leucocyte kit (Sigma, St. Louis, MO). After the sections had been rehydrated and washed, they were incubated in a solution of naphthol AS-BI phosphoric acid and fast garnet GBC for 1 h at 37°C. Nuclei were counterstained with haematoxylin. TRAP-positive cells that were dark red to purple in colour and contained two or more nuclei were considered as osteoclasts.

For gene expression analysis by qRT-PCR five recovered implants were rapidly frozen on dry ice and stored at -80°C until use. Samples were homogenized using a cryogenic mill (6770 Freezer/Mill®, SPEX® SamplePrep, Metuchen, NJ, USA) and total RNA was extracted with a phenol-chloroform method using TRIzol reagent (Life Technologies) and processed as described for *in vitro* samples. Specific primers for mouse and sheep genes were purchased from IDT (Supporting information, Table S2). The expression of genes of murine or ovine origin was analyzed separately. Gene expression was normalized to *GAPDH* and results are reported as $-\Delta Ct$. One-way ANOVA followed by the Bonferroni test for multiple comparisons was performed to analyze the differences among the three different particle sizes in DBM group and in MSC-seeded

DBM group. Unpaired t-test was used to compare differences between DBM and corresponding MSC-seeded DBM implants for each particle size.

RESULTS

DBM characterization

Radiographic images, performed before and right after the demineralization process, confirmed that all DBM samples were demineralized (Supporting information, Fig. S1). To verify that each DBM sample contained particles of the expected size, HR-SEM was performed and manual measurements carried out on acquired images. Each sample contained random polygonal spindle shapes in particles of following sizes: 1 mm- mm (DBM-L), 0.5 mm-1 mm (DBM-M), and < 0.5 mm (DBM-S) [Fig. 1(A)].

Calcium removal was quantitatively evaluated after demineralization protocol. As revealed by ICP-OES (Supporting information, Table S3) and confirmed by DTA (data not shown), the percentage of Ca content decreased in the samples after the demineralization procedure. In DBM-L, DBM-M and DBM-S fractions, the percentage of Ca content was less than 0.5%, confirming the efficiency of the procedure.

The FTIR spectra of bone particles before the demineralization exhibited all the most intense bands observed in the spectrum of apatite (at 500-700 cm^{-1} and 900-1200 cm^{-1}) and that of collagen (in the 1200-1700 cm^{-1} and 2800-3700 cm^{-1} regions), being nearly coincident with the sum of the individual profiles [Fig. 1(B)]. Nevertheless, there were some bands (namely at around 870 cm^{-1} and 1400-1450 cm^{-1}) that originated from carbonate substitutions in the crystal lattice of apatite. The most intense bands originated in the mineral phase, in accordance with its larger proportion in the composite. In particular, the bands at 564 and 599 cm^{-1} correspond mainly to $PO4^{3-}$ bending vibrations, despite some minor contribution from collagen (amide bands) in that region. Moreover, the absorptions at 1102 and 1026 cm^{-1} corresponded to the symmetric and asymmetric stretching of phosphate, respectively. On the other hand, the collagen showed the typical Amide I and Amide II bands at 1656 and 1553 cm^{-1}, respectively. Furthermore, the bands at 1420 and 1460 cm^{-1}

correspond to absorptions from CH_2 wagging and bending vibrations superimposed with those from asymmetric stretching vibrations of CO_3^{2-} groups, present as ionic substitutes in the apatite crystal. Carbonate also originates a band at ca. 870 cm^{-1}, which was assigned to the bending vibration. The spectra related to the DBM-L, DBM-M and DBM-S samples, in comparison with the sample of bone before demineralization, highlight the complete disappearance of phosphate bending and stretching vibrations bands, while the characteristic bands of the collagen are present, showing efficiency of the demineralization procedure [Fig. 1(B)]. However, if we observe the maxima of the characteristic peaks of the collagen in the demineralized samples, in comparison with the spectra of the native bone, the peaks of the Amide I and Amide II shift to lower wavenumber (cm^{-1}) especially in the DBM-S sample where the Amide II band are missing. These data suggested that the same procedure of demineralization, used on the three samples, had a different effect on the secondary structure of the collagen according to the different size of the DBM particle. When using the smallest particles (DBM-S), we observe an especially strong change in the secondary structure of collagen.

The X-Ray diffraction (XRD) pattern of bone particles before the demineralization showed the characteristic diffraction maxima of an apatite single crystalline phase [Fig. 1(C)]. After the demineralization, the XRD patterns showed the loss of crystalline structure, indicating a complete demineralization of the bone for all three DBM samples. The XRD patterns also highlight the peak around 7.5° 2 theta and a large broadening amorphous peak at about 25° 2 theta corresponding to the collagen structure. In addition, the profile of DBM-M shows an increase of the amorphous and collagen peaks compared to DBM-L, while the profile of DBM-S's amorphous peak appears broader while the peak of the collagen decreases, likely due to loss of the structure of the collagen.

DTA was used to evaluate the quantitative and qualitative composition of the bone particles before and after the demineralization procedure. Figure 1(D) shows the comparison of DTA analysis of the three particle samples before the demineralization and after the grinding (fraction 1-L; fraction 2-M; fraction 3-S) in order to evaluate the grinding effect on both organic and inorganic matter of the

native bone. Three main stages of weight loss were observed in all three bone fractions before demineralization. The first one was due to water evaporation of the main mass around 90 °C which corresponds to an endothermic process. The second weight loss derived from the decomposition of collagen and other residual organic components.[27] The third weight loss, above 800 °C, matches mostly to the fraction of hydroxyapatite as the inorganic constituent. These results are evidence that the grinding of the bone damages the crystalline structure of the apatite while the collagen does not undergo significant change. After demineralization, DTA performed on all three samples revealed the absence of the peak at about 867 °C, confirming the complete demineralization of the bone independent of particle size [Fig. 1(E)]. Moreover, we observe a different thermal stability of the organic matrix in relation to different particle size of the DBM fractions. The peaks of the decomposition of collagen and other residual organic components shift at lower temperature respect to the bone before demineralization. Comparing the three thermogram of the DBM-L, DBM-M and DBM-S samples, we observed that degradation temperature of DBM-S's collagen (peaks at 323.72 °C) was higher than DBM-L (peak at 318.82 °C) and DBM-M (peak at 319.26 °C). The thermogram of the DBM-L highlighted indeed three peaks of the degradations of no-collagen organic matrix (peak at 206.41 °C, 226.72°C and 248.17 °C respectively), while the thermogram of DBM-M showed a single peak of non-collagen organic matrix at 206.41 °C.

Overall, DTA analysis highlights a relationship between particle size and DBM quality. In the smallest particles (DBM-S) the process of demineralization resulted in a deterioration of both collagen and non-collagen organic molecules.

DBM cytocompatibility

Cell seeding efficiency and metabolic activity

To investigate whether bone marrow derived MSC adhere to the DBM particles of different sizes, we quantified the cell-seeding efficiency (CSE). The data revealed a significant efficiency rate for all the four seeding densities and for all the three particle sizes [Fig. 2(A)]. A CSE > 90% was found in all conditions, but DBM-M showed better seeding efficiency compared to DBM-L (on

average + 6.1%) and DBM-S (on average + 3.2%) although the difference was statistically significant only when compared to DBM-L. Only at the seeding density of 8×10^5 cells did the particle size have no effect on CSE. The CSE was 95%, 97.7%, and 94.5% for DBM-L, DBM-M, and DBM-S, respectively.

In order to measure whether DBM particle size could affect cellular metabolism, an Alamar Blue assay was performed on cell-seeded DBM at day 1 and day 3 of culture [Fig. 2(B)]. Our results demonstrate that MSC maintain a metabolically active state when seeded on all the three DBM samples at the indicated cell seeding numbers. Nevertheless MSC seeded on DBM-M displayed higher metabolic activity compared to DBM-L and DBM-S under most of the cell concentrations tested, although not in a statistically significant manner.

Given that the seeding concentration of 8×10^5 cells provided the best balance between cellular adhesion and metabolic activity, this concentration was selected for the successive experiments.

Cell morphology, distribution and viability

The effect of DBM particle size on cell morphology was evaluated during time in culture by HR-SEM [Fig. 3(A)]. At day 1 of culture the spindle-shaped MSC were distributed along the particles independently of size. After 3 days of culture on DBM particles, there were many spreading cells in physical contact with each other forming a dense cell layer and covering most of the particle surface. Overall, HR-SEM images show that the particle size did not affect cell morphology and cell-to-cell contact behavior.

We further evaluate cell viability and distribution at days 1 and 3 of culture by using the Live/Dead staining kit and by imaging with confocal laser microscope [Fig. 3(B)] and fluorescence microscope [Fig. (4)]. MSC seeded on the three DBM fractions were mostly viable at day 1 as well as day 3 with only few dead cells, indicating a high rate of cellular viability for the three particle sizes. Interestingly, the distribution of the cells was instead influenced by the particle size. MSC were distributed on the most particle's surface on DBM-M compared to DBM-L, which in turn was better

than DBM-S where they appeared unevenly distributed. This feature was evident at day 1 of culture and was more pronounced after 3 days of culture.

DBM osteoinductivity

To evaluate the effect of particle size on the *in vitro* osteogenic potential of DBM, MSC were cultured with DBM fractions and analyzed for specific genes' expression and mineralization [Fig. (5)]. Relative gene expression of bone markers was calculated using MSC grown in αMEM containing 2% FBS without any DBM fraction as calibrator (CRL sample). Quantitative RT-PCR performed at day 2 and day 6 of DBM exposure showed no significant difference in the expression of *COL1A1* in comparison to control condition (data not shown). Conversely, *RUNX2* expression was significantly downregulated in DBM-L, DBM-M, and DBM-S at both day 2 (mean fold change = 0.26, 0.27, and 0.45, respectively) and day 6 (mean fold change = 0.56, 0.46, and 0.76, respectively) [Fig. 5(A)]. The level of osteocalcin (*BGLAP*), a direct target of *RUNX2*, was significantly upregulated at day 2 in DBM-S samples (mean fold change = 10.69), while at day 6 the expression level significantly increased in DBM-L, DBM-M, and DBM-S (mean fold change = 57.81, 49.26, and 38.42, respectively) [Fig. 5(B)]. The mineralization assay performed by Alizarin Red staining revealed the presence of a mineralized matrix starting at day 6 and becoming more evident at day 13. The Alizarin Red staining appeared weaker in DBM-S at day 6 compared to DBM-M and DBM-L while at day 13 it was comparable in all three DBM fractions [Fig. 5(C)]. We hypothesize that *RUNX2* upregulation occurred at a very early time point (< 2 days), because we observed its downstream effects: *BGLAP* modulation (since day 2) and mineralization (since day 6). In order to confirm the osteogenic potential and the possible effect of the particle size, the three DBM samples were subcutaneously implanted into athymic mice. Table 1 summarizes the histological findings of DBM-associated osteogenesis performed on retrieved implants after 8-week implantation. We found that particle size influences the DBM osteogenic potential. In particular, when DBM was implanted without cells, only DBM-M particles demonstrated a positive incidence of new bone formation (40%), while DBM-L and DBM-S alone showed no bone formation. MSC-

seeded DBMs demonstrated an incidence of positive implants of 40%, 80%, and 80% for DBM-L, DBM-M, and DBM-S respectively. Therefore, particle size also influences the osteogenic potential of MSC-seeded DBM particles, primarily the medium and small particle sizes.

Figure 6 shows representative sections from the six experimental groups (DBM-L, DBM-M, DBM-S alone or seeded with MSC). DBM particles differ from the connective tissue since particles are characterized by a lamellar structure. Non-seeded DBM particles appeared associated with loose connective tissue and several blood vessels are visible. When DBM particles were not seeded with MSC, the newly formed bone is visible only in DBM-M group with presence of polar and slightly rounded cells that reside in lacunae [Fig. 6(A)]. In all cases absence of inflammation and occasional tissue ingrowths with fibroblasts lying in close proximity to DBM is present. In MSC-seeded DBM particles, new bone formation was visible in all three DBM fractions, but with different incidence. H&E images [Fig. 6(A)] show several areas of homogenous osteoid matrix adjacent to MSC-seeded DBM particles. New woven bone is distinguishable from DBM particles by the presence of cuboidal osteoblast-like cells lining the surface of the newly formed bone, and of osteocytic cells strictly incorporated within the new bone tissue, contrary to the decellularized lamellar bone structure typical of DBM. The osteoid areas are characterized by a condensations of collagenous fibers, as evident at higher magnification. Loose connective tissue and blood vessels are evident also in MSC-seeded DBM explants. Masson trichrome and toluidine blu/fast green stains analyses also confirmed these results. Masson trichrome stain [Fig. 6(B)] exhibit dark blue staining for collagen deposition, indicative of bone formation, in particular in MSC-seeded DBM-M and DBM-S samples. In MSC-seeded DBM-M sections, new bone in direct apposition along the DBM granules was observed as well as the presence of numerous osteocytes within the newly formed bone. Finally, marginal resorption of DBM granules and cell invasions are also evident in MSC-seeded DBM-M samples. Presence of newly formed bone and osteoid matrix strictly adjacent to MSC-seeded DBM-M and DBM-S particles are also confirmed by violet staining of toluidine blu/fast green stain [Fig. 6(C)]. 8 weeks after DBM implantation, copious TRAP-positive

multinucleated cells adhered to DBM-M and DBM-S particles seeded with MSC were detectable [Fig. 8], thus suggesting that these cells are osteoclasts that can resorb DBM. Osteoclasts are present not only in the peripheral region but also in the central region of the implanted area. These results show that new bone formation is coupled with bone resorption of the DBM particles, in particular in DBM-M samples. Contrary to the plentiful presence of osteoclasts seen in MSC-seeded DBM-M and DBM-S, in MSC-seeded DBM-L samples no TRAP-positive multinucleated cells were detected (data not shown).

To further understand if the cellular contribution to the new formed bone derived from sheep MSC or from the cells of the host, a gene expression analysis was performed by qRT-PCR using specific sheep and mouse primers in recovered implants. The sheep gene expression was carried out on MSC-seeded DBM explants. The expression of sheep genes in recovered implants 8 weeks after subcutaneous implantation within athymic mice was barely detectable. In the MSC-seeded DBM-L group, 75% of samples did not display any expression of the reference gene *GAPDH* nor the selected genes, whereas MSC-seeded DBM-M and -S recovered implants show low levels of expression of analyzed genes, with no significant differences between the two groups (data not shown).When comparing the effect of particle size in DBM and in MSC-seeded DBM groups, no differences were observed in mouse *Col1a1* or *Vegfa* expression (data not shown). Instead, both the transcript levels of mouse *Bglap* (Osteocalcin) and *Tnfsf11* (RANKL) were significantly lower in the DBM-S group with respect to the DBM-M and DBM-L groups ($^{\circ}p<0.05$), while the particle size did not influence the expression of either *Bglap* and *Tnfsf11* when MSC were seeded on the particle before implantation [Fig. 8 (A,B)]. Comparing the effect of MSC in each size of DBM particles, we found that the expression of mouse *Bglap* was lower in MSC-seeded DBM-L ($*p<0.05$) and -M ($**p<0.01$) compared to the counterparts without cells, but higher in MSC-seeded DBM-S with respect to DBM-S ($*p<0.05$) [Fig. 8(A)]. Mouse *Tnfsf11* expression was lower

in MSC-seeded DBM-L (*$p<0.05$) and -M (**$p<0.001$) compared to the relative DBM without cells [Fig. 8(B)].

DISCUSSION

Demineralized bone matrix (DBM) is a versatile collagen-based biomaterial extensively used in orthopaedic repair and regenerative medicine contexts, but there are conflicting reports in the literature on the efficacy of this product. Among the relevant features that determine the variability of DBM osteoinductivity, particle size is often poorly evaluated and considered differently among several published works. Furthermore, to our knowledge, it has not been paid attention to what is altered in bone matrix throughout the DBM manufacturing procedure in order to understand where variability lies, and try to elucidate how to standardize DBM manufacturing. In the present work we describe how DBM preparation affect collagen, which is the major component of extracellular matrix and plays a pivotal role in supporting the attachment and proliferation of multipotent stromal cells.[28,29] Here, we produced sheep DBM particles to explore the effect of particle size on collagen structure. Using three different particle sizes, our data showed that the demineralization process affect collagen structure in relation to particle size. We found that the size-dependent alteration of collagen influences DBM cytocompatibility and in *vivo* osteoinductivity. To best of our knowledge, this is the first evidence that changes on collagen structure induced by demineralization have a biological effect, and this information is crucial as it should contribute to DBM manufacturing standardization.

Prior to clinical application, a novel treatment needs to be evaluated in a preclinical, large animal model. Sheep is the elective model for orthopaedic and trauma related research. We thus produced and characterized DBM from sheep cortical bone to be used for future *in vivo* efficacy studies using sheep as animal model and to overcome the species limitation found when xenogenic materials are used.[30] A detailed chemical-physical characterization of three DBM samples with different sizes was conducted. The XRD profiles performed after demineralization show in all samples the absence of the mineral apatite component and broad peaks typical of collagen proteins. We detected two

diffraction peaks at the diffraction angles (2θ) of about 7.5˚ and 25˚, respectively sharp and wide, in accordance with the characteristic diffraction peaks of collagen, meaning that this protein displays an ordered structure or an ordered structure snippet. However, the XRD profile of the smallest particles, DBM-S, show a decreased peak intensity and more peak broadening that may be due to a modification of the diameter of the tri-helix collagen molecule and the single left-hand helix chain. These results were also confirmed by FTIR and TGA analyses. Through FTIR analysis we observe that the peak of the Amide I (1658 cm^{-1} for native bone and 1635 cm^{-1}, 1637 cm^{-1}, 1624 cm^{-1} for DBM-L, DBM-M, and DBM-S respectively) progressively shifts to lower wavenumbers (cm^{-1}) from the largest to smallest particles. The peak of Amide II (1551 cm^{-1} for native bone and 1557 cm^{-1}, 1560 cm^{-1} for DBM-L, and DBM-M respectively, no peak observed for DBM-S) shifts to higher wavenumbers (cm^{-1}) from the largest to medium particles, while it disappears in the smallest particles. As demonstrated by Iafisco et al.,[31] a shift of the Amide I band to lower wavenumbers corresponds to a reduction of the ordered β-sheet and an increase in the random and β-turn structures. This means that the procedure to obtain DBM induces alterations to collagen structure in a size-dependent manner, remarkably in the smallest particles. In addition, we analyzed bone particles before and after demineralization in order to elucidate separately the effect of grinding and demineralization. DTA analysis showed a change in thermal stability of the degradation peaks of the collagen and the loss of the mineral matrix in all demineralized samples with respect to the non-demineralized bone. In demineralized bone particles the peak of the degradation of collagen shifts at lower temperatures in a size-dependent manner with respect to non-demineralized bone particles. The analysis of bone particles before demineralization highlights that the grinding of the native bone induces a modification of the crystalline structure of the apatite. In fact, we observe a shift of the peak, in the range 800-900 °C, with regards to the three different particles size fractions obtained by grinding: 874 °C, 881° C and 868°C for fraction L, M, and S, respectively. After grinding (before demineralization), no change in the structure of the collagen was observed. Overall

the chemical-physical characterizations highlighted a relation between DBM particle size and structural modification of the collagen that can be ascribed to the demineralization process.

To verify whether the size-dependent alteration of collagen might affect cytocompatibility, we analysed MSC behaviour once cultivated onto or in contact with DBM particles *in vitro*. It is known that collagenous matrix provides a suitable substratum for anchorage-dependent survival, proliferation and differentiation of cells that are involved in tissue repair.[30,32–34] Our study demonstrates that cell seeding efficiency of MSC onto all DBM fractions was good overall, although DBM-M particles had a higher cell adhesion compared to DBM-L and DBM-S particles. Given that smaller particles expose more surface, the expected result in the cell seeding assay would have been DBM-S>M>L. However, the obtained result is DBM-L<M>S, which makes one think that the molecules that mediate cell adhesion have been more altered with demineralization in small particles compared to medium particles, as it happens to collagen. Fibronectin, beyond collagen, is an essential component of the extracellular matrix and is a key player in different cellular processes, including adhesion. It has been demonstrated the importance of the fibronectin-collagen interaction in the cell adhesion and the molecular details of the fibronectin-collagen interaction have been elucidated.[35] This thought gets stronger with the observation of fluorescence microscopy images. MSC appearance and morphology did not differ among the distinct particle sizes, as demonstrated by SEM, whereas fluorescence microscopy analysis revealed a better cell distribution and growth on DBM-M compared to DBM-L and DBM-S particles. An active cell metabolism was detected in all DBM particles, although the metabolic activity of MSC was slightly higher on DBM-M particles. Overall, in our *in vitro* assays we found the best results in terms of MSC adhesion, metabolic activity, and distribution for DBM particles of medium size with an “intermediate” grade of collagen modification.

The effect of size-dependent alteration of collagen on DBM osteoinductivity was then analyzed. *In vitro* gene expression analysis of MSC cultured in contact with DBM-L, -M, and -S showed a decrease of *RUNX2* levels and a strong upregulation of *BGLAP*. *RUNX2* is the master regulator of

osteogenic differentiation and it is upregulated in early osteogenic commitment, but afterwards it has to be downregulated in order to permit late differentiation and mineralization.[36] *BGLAP* is a direct target of *RUNX2* and encodes for osteocalcin, a late osteogenic marker and a regulator of the mineralization process. These results, combined with the formation of a mineralized matrix detected by Alizarin Red staining, demonstrated that DBM particles can induce MSC osteogenic differentiation *in vitro* without adding any supplemental differentiation agents, and that particle size did not significantly affect the outcome. In addition, DBM osteoinductive potential was evaluated in a mouse ectopic subcutaneous model. The subcutaneous ectopic model is extremely selective when evaluating the scaffold's intrinsic osteoinductive abilities, since eliminates the contribution of endogenous osteogenic stimuli.[37] When we implanted DBM particles alone, we found osteoinductive ability only for DBM-M group. No implant that was positive for bone formation was found in DBM-L and DBM-S groups 8 weeks after ectopic implantation. In agreement, DBM particles ranging from 500 to 1000 μm have been shown to provide the best incidence of new bone induction in rats.[16] To our knowledge, this is the first time that the *in vivo* results can be explained by the chemical-physical characterization of DBM particles, highlighting a relation between DBM particle size, structural modification of the collagen, and osteoinductivity *in vivo*. In our study the medium particles (DBM-M) represent a good compromise between no modification (largest particles, DBM-L) and excessive modification (smallest particles, DBM-S) of collagen structure, yielding highest osteoinductive ability. Even if the precise role of the collagenous matrix in bone induction is not yet fully elucidated, several studies suggest that modified matrix proteins can influence cell localization and function. For example RAW 264.7 and the J774.1 murine macrophage cells adhered remarkably well when cultured on denatured conformations of type I collagen instead of native collagen.[38] Another important factor believed to be crucial to osteoinduction is the diffusion of matrix-associated growth factors, such as bone morphogenetic proteins (BMPs), from DBM into the surrounding tissue. BMP's release into the host implant site seems to be more important than their content in DBM. Sampath and Reddi[17] demonstrated that

subcutaneous implantation of rat DBM induced new bone formation only when a coarse powder was used (74-4 0 μm), whereas no induced bone was observed using a fine matrix (44-74 μm). However, the fine matrix extract in addition to inactivated coarse matrix lead to the complete restoration of biological activity in inactive coarse matrix. These results demonstrate that although fine bone matrix holds osteoinductive proteins, matrix size is an important factor in triggering the biochemical cascade of endochondral bone differentiation. Furthermore, it was demonstrated that the release kinetics of BMP-7 from bovine DBM in a physiological buffer solution is a function of DBM particle size.[39] These published results demonstrated a relation between DBM particle size and diffusion of matrix-associated osteoinductive proteins. An interesting aspect to be investigated in further studies is the possible relation between DBM collagen structure and the release kinetics of BMPs from DBM particles.

In a tissue engineering approach, cells are added to bone-graft substitutes in order to improve their osteogenic potential. We evaluated if size-dependent alteration of collagen influences *in vivo* DBM osteoinductivity when MSC are seeded onto DBM particles one day before implantation. We found that all MSC-seeded DBM particles induced new bone formation when subcutaneously implanted, indicating an efficient contribution of MSC to DBM regardless the size of the particles. In particular, MSC seeded DBM-L, -M and -S particles showed 40%, 80% and 80% of implants that were positive for bone formation, respectively, compared to 0%, 40%, and 0% of corresponding DBM particles without cells. These results are in agreement with data in literature where multipotent adult progenitor cells enhanced DBM osteoinductivity.[40,41] New bone formation is coupled with bone resorption of the DBM particles, in particular in DBM-M samples, as evidenced by TRAP staining. Finally, the data from gene expression analysis performed on recovered implants showed that mouse *Bglap* and *Tnfsf11* levels were lower in MSC-seeded DBM explants than in DBM explants of corresponding particle size, explaining the higher incidence of bone formation in MSC-seeded DBM groups. Bglap encoded for osteocalcin. Despite being a late osteogenic differentiation marker, its biological role as a protein is to inhibit bone mineralization

through its Gla domain.[42] Therefore, we believe that Bglap lower level revealed 8 weeks after implantation may reflect a higher mineralization level in MSC-seeded DBM groups. Since Tnfsf11 encodes for RANKL, a powerful stimulator of osteoclastogenesis, its lower level in MSC-seeded samples may indicate a lower level of osteoclastogenesis. Even though sheep-derived RNA was barely detectable in all explants after 8 weeks from implantation, the differences observed in murine gene's expression indicate that sheep MSC improve the osteoinductivity of DBM by regulating the host osteoprogenitor cells through a paracrine effect.

CONCLUSION

This study demonstrates that DBM collagen structure is affected by particle size. The chemical-physical characterization shows a particle size-dependent alteration in collagen structure, with medium particles being altered but not as much as small particles. The collagen alteration found in medium particles is likely the best condition for cytocompatibility *in vitro* and for bone induction *in vivo* in comparison to no alteration found in large particles and deterioration found in small particles. The use of medium (0.5-1 mm) particles *in vivo* is preferable when DBM is implanted alone, while medium and small (< 0.5 mm) particles are recommended when DBM is implanted in association with MSC. Therefore, we identified in the collagen structure a key variable to consider as a relevant feature that can influence DBM osteoinductivity. This information is crucial as it should contribute to DBM manufacturing standardization.

We hope our results will guide researchers to use DBM particles of 0.5-1 mm size range in bone tissue-engineering applications. This will enable researchers to obtain results more comparable and reliable among different research groups. Furthermore, the prior analysis of collagen structure can guide in the selection of DBM particles to be used to induce new bone formation allowing a reduction of animals used to test osteoinductivity in according to 3R principle.

Our future research will test whether DBM medium particles support the repair of a critical bone defect in a sheep model, eventually leading to improved therapies for clinical skeletal reconstruction.

ACKNOWLEDGMENTS

Research reported in this publication was supported by Istituto Zooprofilattico Sperimentale della Lombardia e dell'Emilia Romagna "Bruno Ubertini" (IZSLER), Brescia, Italy. The authors wish to thank Dr. Marco Gambarotti for his precious help on histological analysis, Dr. Gabriella Teti for her assistance with scanning electron microscopy, Charlotte Mcilwaine Story and Emily Aharon for editorial assistance.

REFERENCES

1. Giannoudis PV, Dinopoulos H, Tsiridis E. Bone substitutes: an update. Injury 2005;36 Suppl 3:S20–7.
2. De Long WG, Einhorn TA, Koval K, McKee M, Smith W, Sanders R, Watson T. Bone grafts and bone graft substitutes in orthopaedic trauma surgery. A critical analysis. J Bone Joint Surg Am 2007;89:649–58.
3. Campana V, Milano G, Pagano E, Barba M, Cicione C, Salonna G, Lattanzi W, Logroscino G. Bone substitutes in orthopaedic surgery: from basic science to clinical practice. J Mater Sci Mater Med 2014;25:2445–61.
4. Kolk A, Handschel J, Drescher W, Rothamel D, Kloss F, Blessmann M, Heiland M, Wolff KD, Smeets R. Current trends and future perspectives of bone substitute materials - from space holders to innovative biomaterials. J Craniomaxillofac Surg 2012;40:706–18.
5. Kurien T, Pearson RG, Scammell BE. Bone graft substitutes currently available in orthopaedic practice: the evidence for their use. Bone Joint J 2013;95:583–97.
6. Laurencin C, Khan Y, El-Amin SF. Bone graft substitutes. Expert Rev Med Devices 2006;3:49–57.
7. Habibovic P, de Groot K. Osteoinductive biomaterials--properties and relevance in bone repair. J Tissue Eng Regen Med 2007;1:25–32.
8. Gruskin E, Doll BA, Futrell FW, Schmitz JP, Hollinger JO. Demineralized bone matrix in bone repair: history and use. Adv Drug Deliv Rev 2012;64:1063–77.
9. Urist MR. Bone: formation by autoinduction. Science 1965;150:893–9.
10. Mauney JR, Jaquiéry C, Volloch V, Heberer M, Martin I, Kaplan DL. In vitro and in vivo evaluation of differentially demineralized cancellous bone scaffolds combined with human bone marrow stromal cells for tissue engineering. Biomaterials 2005;26:3173–85.
11. Fleming JE, Cornell CN, Muschler GF. Bone cells and matrices in orthopedic tissue engineering. Orthop Clin North Am 2000;31:357–74.
12. Zhang M, Powers RM, Wolfinbarger L. Effect(s) of the demineralization process on the osteoinductivity of demineralized bone matrix. J Periodontol 1997;68:1085–92.
13. Han B, Yang Z, Nimni M. Effects of moisture and temperature on the osteoinductivity of demineralized bone matrix. J Orthop Res 2005;23:855–61.
14. Pietrzak WS, Ali SN, Chitturi D, Jacob M, Woodell-May JE. BMP depletion occurs during

prolonged acid demineralization of bone: Characterization and implications for graft preparation. Cell Tissue Bank 2011;12:81–8.

15. Glowacki J. A review of osteoinductive testing methods and sterilization processes for demineralized bone. Cell Tissue Bank 2005;6:3–12.

16. Syftestad G, Urist MR. Degradation of bone matrix morphogenetic activity by pulverization. Clin Orthop Relat Res 1979;141:281–5.

17. Sampath TK, Reddi AH. Importance of geometry of the extracellular matrix in endochondral bone differentiation. J Cell Biol 1984;98:2192–7.

18. Reddi AH, Huggins C. Biochemical sequences in the transformation of normal fibroblasts in adolescent rats. Proc Natl Acad Sci U S A 1972;69:1601–5.

19. Dozza B, Di Bella C, Lucarelli E, Giavaresi G, Fini M, Tazzari PL, Giannini S, Donati D. Mesenchymal stem cells and platelet lysate in fibrin or collagen scaffold promote non-cemented hip prosthesis integration. J Orthop Res 2011;29:961–8.

20. Zhou X, Holsbeeks I, Impens S, Sonnaert M, Bloemen V, Luyten F, Schrooten J. Noninvasive Real-Time Monitoring by AlamarBlue ® During In Vitro Culture of Three-Dimensional Tissue-Engineered Bone Constructs. Tissue Eng Part C Methods 2013;19:720–9.

21. Impens S, Chen Y, Mullens S, Luyten F, Schrooten J. Controlled Cell-Seeding Methodologies: A First Step Toward Clinically Relevant Bone Tissue Engineering Strategies. Tissue Eng Part C Methods 2010;16:1575–83.

22. Chen Y, Bloemen V, Impens S, Moesen M, Luyten FP, Schrooten J. Characterization and optimization of cell seeding in scaffolds by factorial design: quality by design approach for skeletal tissue engineering. Tissue Eng Part C Methods 2011;17:1211–21.

23. Maddox E, Zhan M, Mundy GR, Drohan WN, Burgess WH. Optimizing human demineralized bone matrix for clinical application. Tissue Eng 2000;6:441–8.

24. Livak KJ, Schmittgen TD. Analysis of relative gene expression data using real-time quantitative PCR and the 2(-Delta Delta C(T)) Method. Methods 2001;25:402–8.

25. Stanford CM, Jacobson PA, Eanes ED, Lembke LA, Midura RJ. Rapidly forming apatitic mineral in an osteoblastic cell line (UMR 106-01 BSP). J Biol Chem 1995;270:9420–8.

26. Minkin C. Bone acid phosphatase: tartrate-resistant acid phosphatase as a marker of osteoclast function. Calcif Tissue Int 1982;34:285–90.

27. Figueiredo M, Cunha S, Martins G, Freitas J, Judas F, Figueiredo H. Influence of hydrochloric acid concentration on the demineralization of cortical bone. Chem Eng Res Des 2011;89:116–24.

28. Yang XB, Bhatnagar RS, Li S, Oreffo ROC. Biomimetic Collagen Scaffolds for Human Bone Cell Growth and Differentiation. Tissue Eng 2004;10:1148–59.

29. El-Jawhari JJ, Sanjurjo-Rodríguez C, Jones E, Giannoudis PV. Collagen-containing scaffolds enhance attachment and proliferation of non-cultured bone marrow multipotential stromal cells. J Orthop Res 2016;34:597–606.

30. Sampath TK, Reddi AH. Homology of bone-inductive proteins from human, monkey, bovine, and rat extracellular matrix. Proc Natl Acad Sci U S A 1983;80:6591–5.

31. Iafisco M, Sabatino P, Lesci IG, Prat M, Rimondini L, Roveri N. Conformational

modifications of serum albumins adsorbed on different kinds of biomimetic hydroxyapatite nanocrystals. Colloids Surf B Biointerfaces 2010;81:274–84.

32. Kleinman HK, Klebe RJ, Martin GR. Role of collagenous matrices in the adhesion and growth of cells. J Cell Biol 1981;88:473–85.

33. Sampath TK, Reddi AH. Dissociative extraction and reconstitution of extracellular matrix components involved in local bone differentiation. Proc Natl Acad Sci U S A 1981;78:7599–603.

34. Popov C, Radic T, Haasters F, Prall WC, Aszodi A, Gullberg D, Schieker M, Docheva D. Integrins α2β1 and α11β1 regulate the survival of mesenchymal stem cells on collagen I. Cell Death Dis 2011;2:e186.

35. Erat MC, Sladek B, Campbell ID, Vakonakis I. Structural analysis of collagen type I interactions with human fibronectin reveals a cooperative binding mode. J Biol Chem 2013;288:17441–50.

36. Bruderer M, Richards RG, Alini M, Stoddart MJ. Role and regulation of RUNX2 in osteogenesis. Eur Cell Mater 2014;28:269–86.

37. Scott MA, Levi B, Askarinam A, Nguyen A, Rackohn T, Ting K, Soo C, James AW. Brief review of models of ectopic bone formation. Stem Cells Dev 2012;21:655–67.

38. Gowen BB, Borg TK, Ghaffar A, Mayer EP. Selective adhesion of macrophages to denatured forms of type I collagen is mediated by scavenger receptors. Matrix Biol 2000;19:61–71.

39. Pietrzak WS, Dow M, Gomez J, Soulvie M, Tsiagalis G. The in vitro elution of BMP-7 from demineralized bone matrix. Cell Tissue Bank 2012;13:653–61.

40. Supronowicz P, Gill E, Trujillo A, Thula T, Zhukauskas R, Perry R, Cobb RR. Multipotent adult progenitor cell-loaded demineralized bone matrix for bone tissue engineering. J Tissue Eng Regen Med 2016;10:275–83.

41. Supronowicz P, Gill E, Trujillo A, Thula T, Zhukauskas R, Ramos T, Cobb RR. Human adipose-derived side population stem cells cultured on demineralized bone matrix for bone tissue engineering. Tissue Eng Part A 2011;17:789–98.

42. Zoch ML, Clemens TL, Riddle RC. New insights into the biology of osteocalcin. Bone 2016;82:42–9.

FIGURE LEGENDS

FIGURE 1. Characterization of bone particles. (A) HR-SEM. Representative images of the demineralized bone particles showing the expected particle size in each fraction: 1mm- mm (DBM-L, large); 0.5mm-1mm (DBM-M, medium); < 0.5mm (DBM-S, small). Scale bar = 100 μm, magnification 60×. Comparison of the FTIR spectra (B) and XRD pattern (C) of bone particles before demineralization and after demineralization (DBM), following the separation in the three size-based samples. Comparison of DTA-TGA profiles from bone samples of three different particle size: (D) before demineralization (fraction 1-L; fraction 2-M; fraction 3-S) and (E) after demineralization (DBM-L; DBM-M; DBM-S).

FIGURE 2. Seeding efficiency and metabolic activity of MSC on DBM particles of three different sizes (L= large; M= medium; S= small). (A) Cell seeding efficiency was performed by an indirect method. After 18 h of contact with 2, 4, 8, or 16 × 10^5 MSC, the cells that did not attach to the particles were quantified and cell seeding efficiency calculated. (B) Metabolic activity of MSC seeded on DBM particles at day 1 and day 3 of culture was evaluated by Alamar blue assay. Data represent mean values ± SD of measurements obtained from MSC isolated from three donors. Each sample was assayed in duplicate. * $p < 0.05$

FIGURE 3. Characterization of MSC cultured on DBM particles of three different sizes (L= large; M= medium; S= small) after 1 and 3 days of culture. (A) HR-SEM images of MSC seeded on DBM particles. Scale bar = 10 μm. (B) Images are representative confocal micrographs showing MSC on DBM particles after Live/Dead cell assay. Viable cells = calcein positive cells, in green. Dead cells= ethiudium positive cells, in red.

FIGURE 4. MSC cultured on DBM particles of three different sizes (L= large; M= medium; S= small). Representative images of fluorescence microscope micrographs showing MSC on DBM particles after 1 day (A) and 3 days (B) of culture *in vitro*. Live/Dead cell assay was used to visualize live cells (calcein positive cells, in green) and dead cells (ethidium positive cells, in red). Scale bar = 200μm.

FIGURE 5. *In vitro* DBM osteoinductivity**.** Osteoinductive effect of addition of DBM particles with three different sizes (L= large; M= medium; S=small) on confluent MSC cultures was evaluated by analyzing specific gene expression and conducting mineralization assays. RUNX2 (A) and BGLAP (B) gene transcription 2 and 6 days after DBM exposition. Data represent mean values ± SD (n=3). CRL= control. * $p<0.05$, ** $p<0.01$ (C) Extracellular matrix deposition and mineralization by MSC exposed to different DBM fractions as revealed by Alizarin Red staining after 6 and 13 days of culture. Scale bar = 200μm.

FIGURE 6. *In vivo* DBM osteoinductivity. DBM samples of three different particle size (DBM-L, DBM-M, and DBM-S), alone or seeded with MSC, were retrieved after subcutaneous implantation in immunocompromised mice for 8 weeks. Recovered implants were stained with haematoxylin and eosin (A), Masson trichrome (B), or toluidine blu/fast green (C). Legend: * blood vessels, # osteoid, § new bone formation, arrowheads point to osteoblasts, arrows point to osteocytes.

FIGURE 7. TRAP staining. Representative photomicrograph of MSC-seeded DBM samples retrieved after subcutaneous implantation in immunocompromised mice for 8 weeks. The multinucleated cells attached to DBM particles (M= medium; S=small) were TRAP-positive. Legend: arrows to TRAP-positive multinucleated cells.

FIGURE 8. Analysis of mouse gene expression in recovered implants following 8-week subcutaneous implantation period. *Bglap* (Osteocalcin) (A) and *Tnfsf11* (RANKL) (B) gene expression was normalized to *GAPDH* and results are reported as $-\Delta Ct$. Differences between three different particle sizes (L= large; M= medium, S= small) in the DBM group and the MSC-seeded DBM group are reported with °. Differences between DBM of each particle size with and without MSC are reported with *. ° $p<0.05$; * $p<0.05$; ** $p<0.01$; n.s. not significance

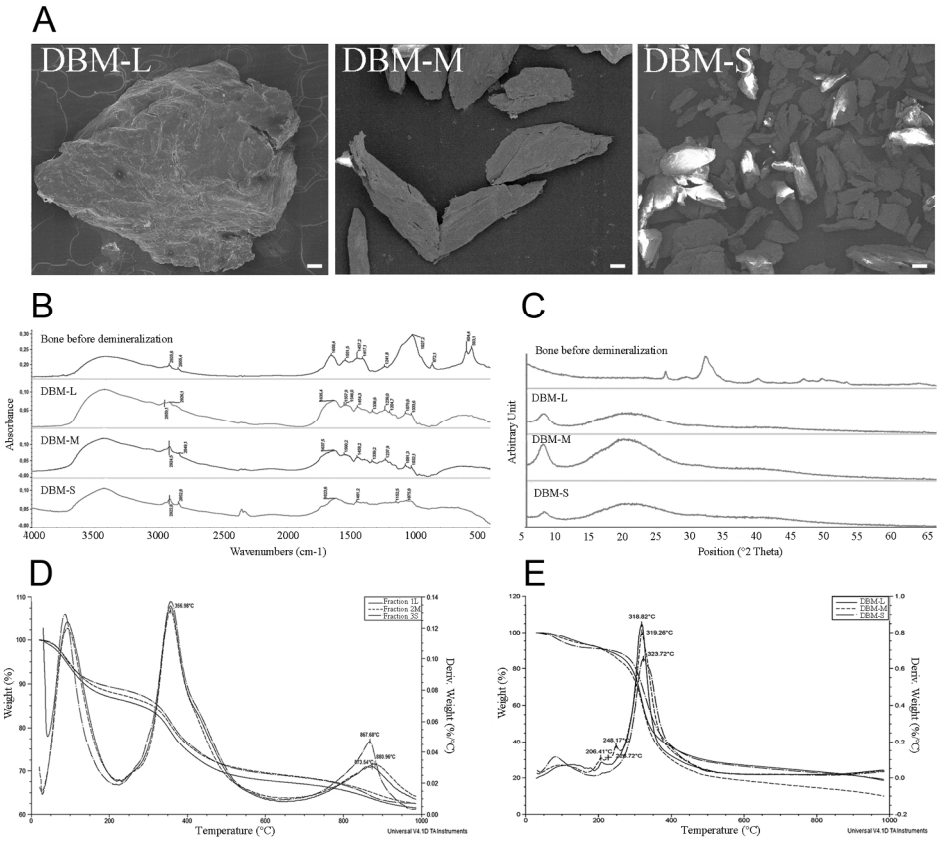

FIGURE 1. Characterization of bone particles. (A) HR-SEM. Representative images of the demineralized bone particles showing the expected particle size in each fraction: 1mm-2mm (DBM-L, large); 0.5mm-1mm (DBM-M, medium); < 0.5mm (DBM-S, small). Scale bar = 100 μm, magnification 60×. Comparison of the FTIR spectra (B) and XRD pattern (C) of bone particles before demineralization and after demineralization (DBM), following the separation in the three size-based samples. Comparison of DTA-TGA profiles from bone samples of three different particle size: (D) before demineralization (fraction 1-L; fraction 2-M; fraction 3-S) and (E) after demineralization (DBM-L; DBM-M; DBM-S).

180x154mm (300 x 300 DPI)

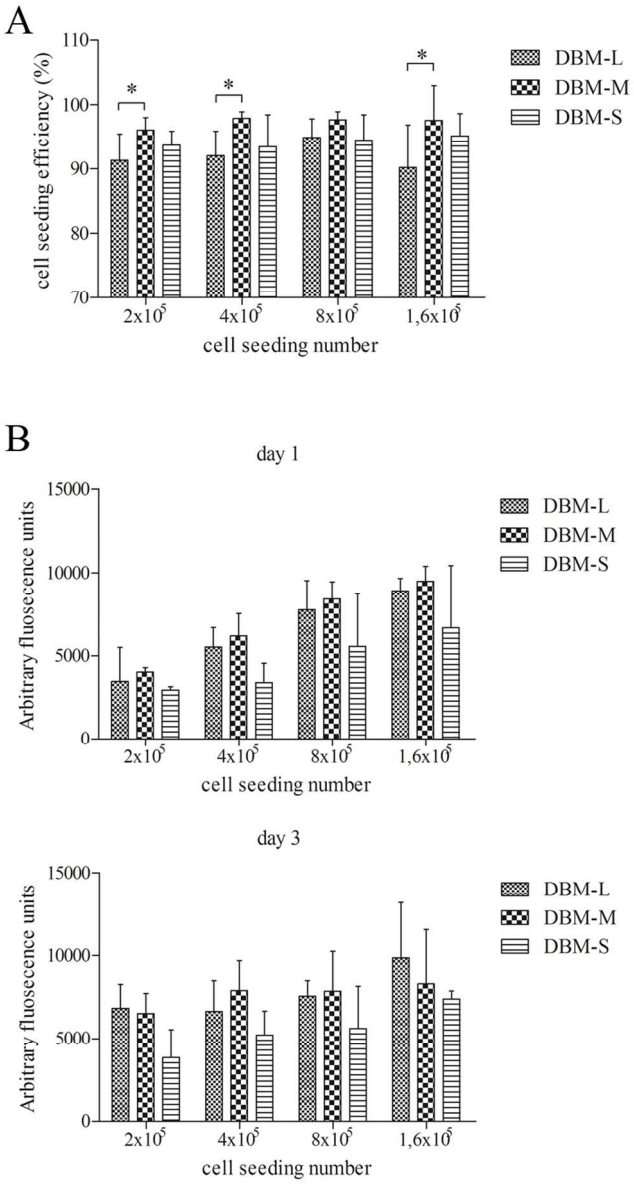

FIGURE 2. Seeding efficiency and metabolic activity of MSC on DBM particles of three different sizes (L= large; M= medium; S= small). (A) Cell seeding efficiency was performed by an indirect method. After 18 h of contact with 2, 4, 8, or 16 × 105 MSC, the cells that did not attach to the particles were quantified and cell seeding efficiency calculated. (B) Metabolic activity of MSC seeded on DBM particles at day 1 and day 3 of culture was evaluated by Alamar blue assay. Data represent mean values ± SD of measurements obtained from MSC isolated from three donors. Each sample was assayed in duplicate. * $p < 0.05$

80x147mm (300 x 300 DPI)

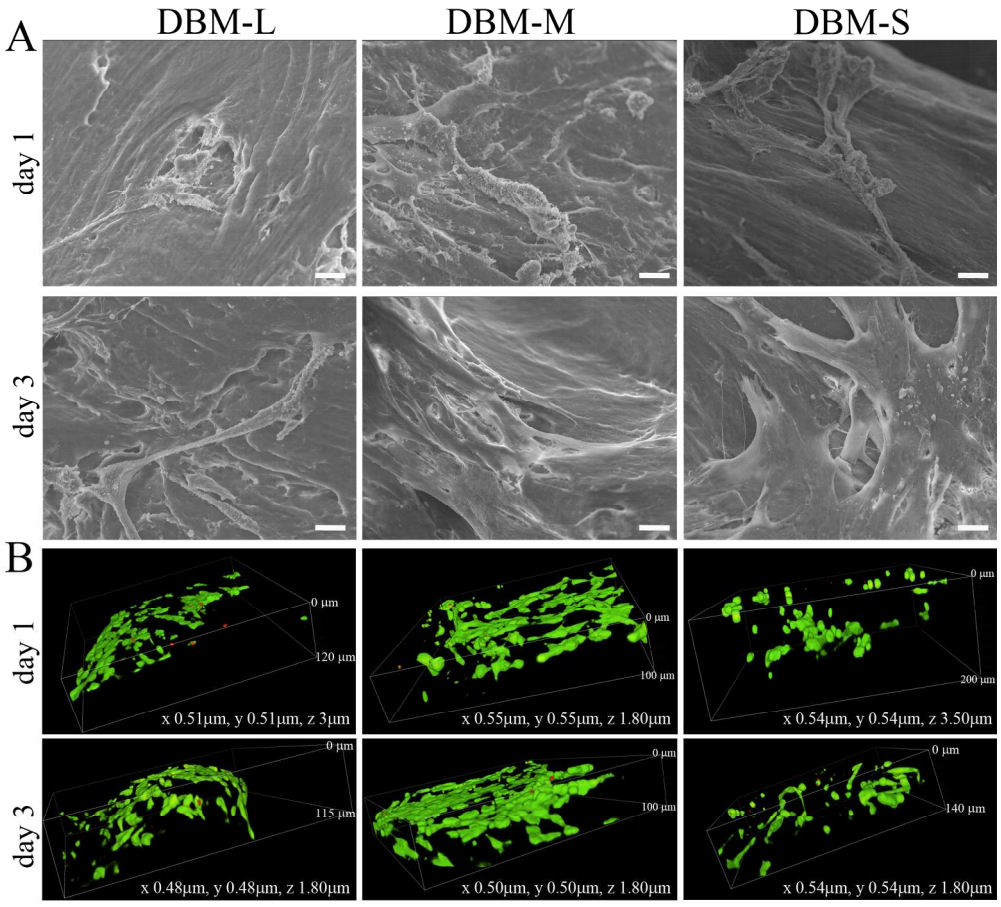

FIGURE 3. Characterization of MSC cultured on DBM particles of three different sizes (L= large; M= medium; S= small) after 1 and 3 days of culture. (A) HR-SEM images of MSC seeded on DBM particles. Scale bar = 10 µm. (B) Images are representative confocal micrographs showing MSC on DBM particles after Live/Dead cell assay. Viable cells = calcein positive cells, in green. Dead cells= ethiudium positive cells, in red.

189x176mm (300 x 300 DPI)

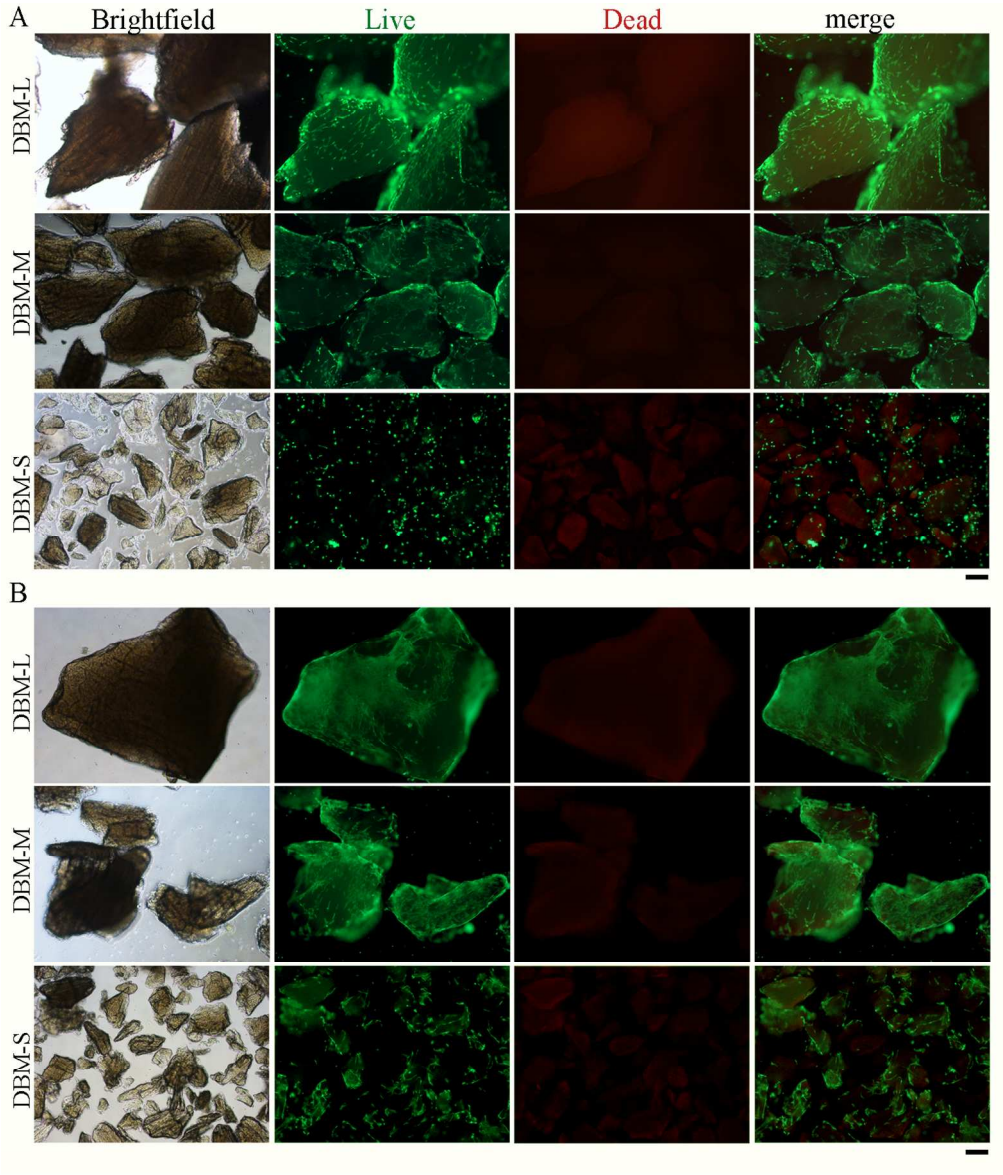

FIGURE 4. MSC cultured on DBM particles of three different sizes (L= large; M= medium; S= small). Representative images of fluorescence microscope micrographs showing MSC on DBM particles after 1 day (A) and 3 days (B) of culture in vitro. Live/Dead cell assay was used to visualize live cells (calcein positive cells, in green) and dead cells (ethidium positive cells, in red). Scale bar = 200μm.

135x158mm (300 x 300 DPI)

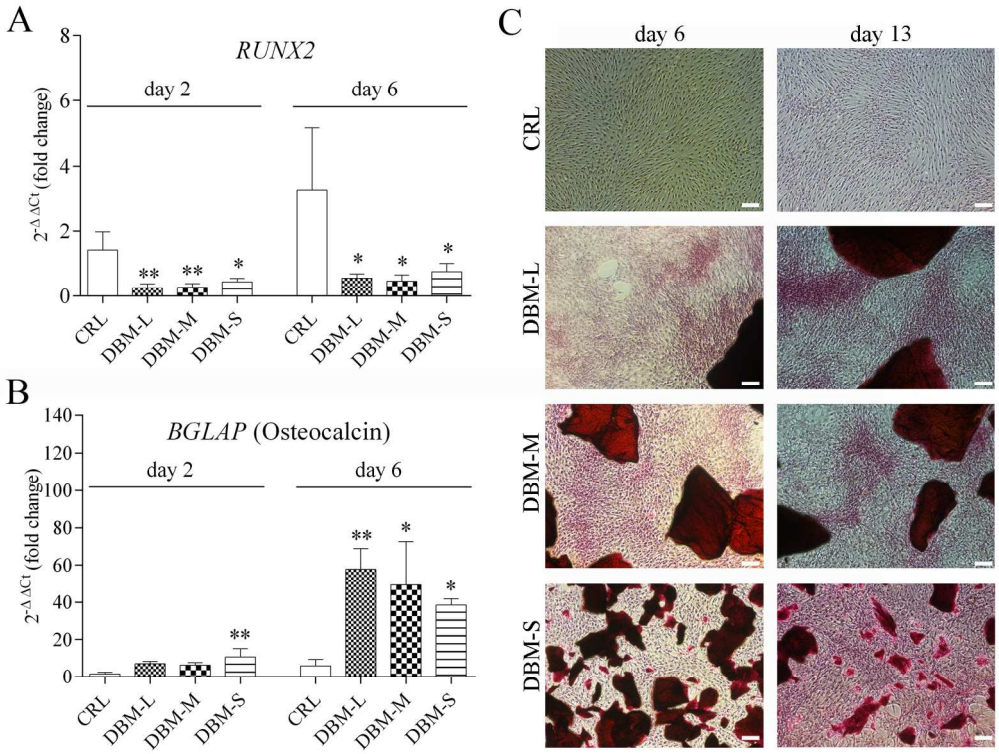

FIGURE 5. In vitro DBM osteoinductivity. Osteoinductive effect of addition of DBM particles with three different sizes (L= large; M= medium; S=small) on confluent MSC cultures was evaluated by analyzing specific gene expression and conducting mineralization assays. RUNX2 (A) and BGLAP (B) gene transcription 2 and 6 days after DBM exposition. Data represent mean values ± SD (n=3). CRL= control. * $p<0.05$, ** $p<0.01$ (C) Extracellular matrix deposition and mineralization by MSC exposed to different DBM fractions as revealed by Alizarin Red staining after 6 and 13 days of culture. Scale bar = 200μm.

170x131mm (300 x 300 DPI)

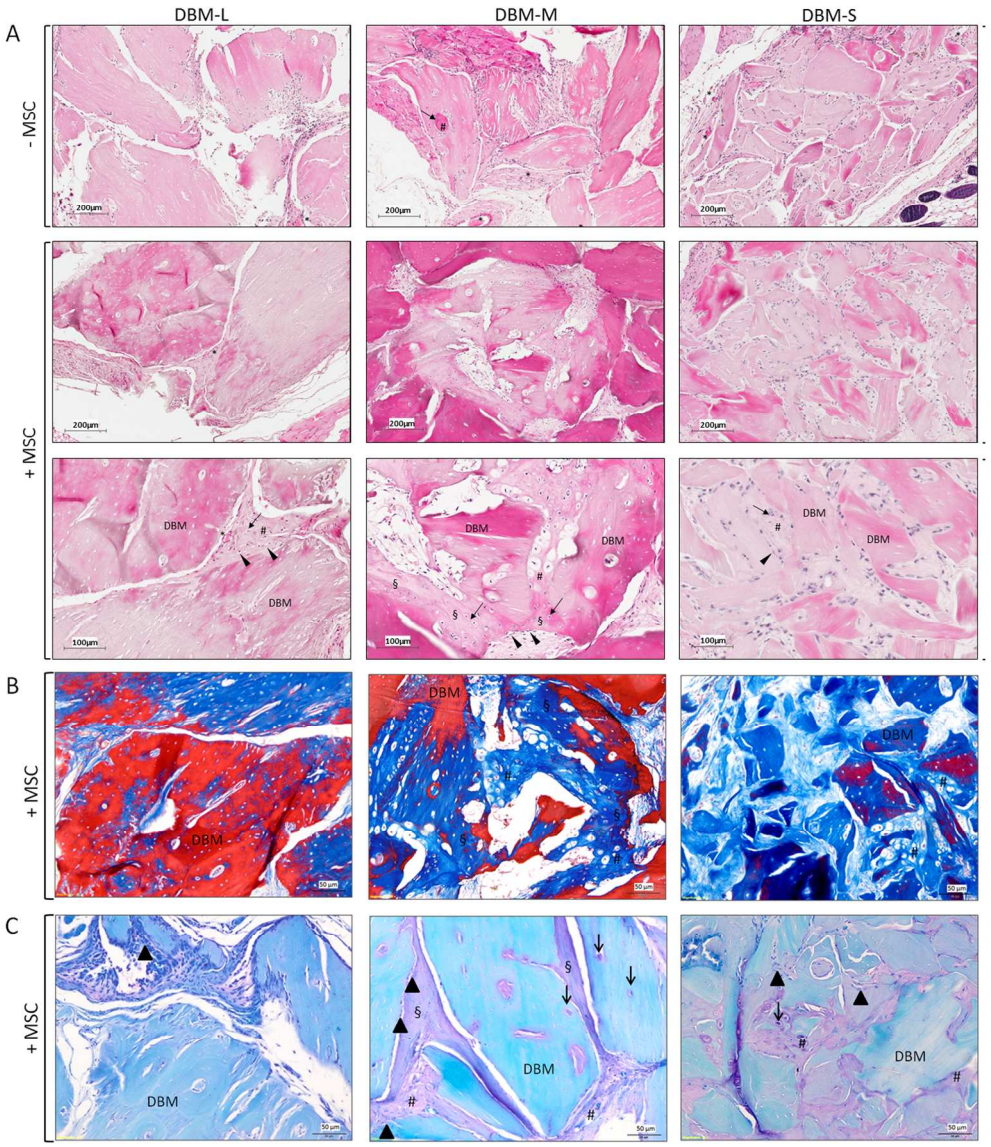

FIGURE 6. In vivo DBM osteoinductivity. DBM samples of three different particle size (DBM-L, DBM-M, and DBM-S), alone or seeded with MSC, were retrieved after subcutaneous implantation in immunocompromised mice for 8 weeks. Recovered implants were stained with haematoxylin and eosin (A), Masson trichrome (B), or toluidine blu/fast green (C). Legend: * blood vessels, # osteoid, § new bone formation, arrowheads point to osteoblasts, arrows point to osteocytes.

156x180mm (300 x 300 DPI)

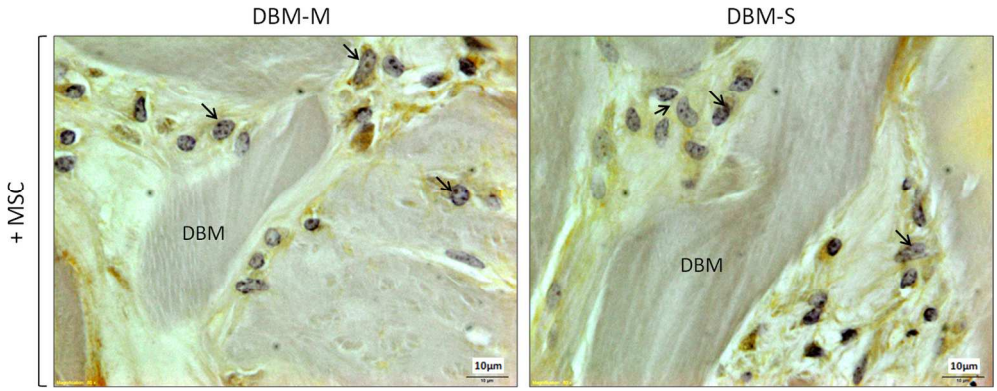

FIGURE 7. TRAP staining. Representative photomicrograph of MSC-seeded DBM samples retrieved after subcutaneous implantation in immunocompromised mice for 8 weeks. The multinucleated cells attached to DBM particles (M= medium; S=small) were TRAP-positive. Legend: arrows to TRAP-positive multinucleated cells.

257x101mm (300 x 300 DPI)

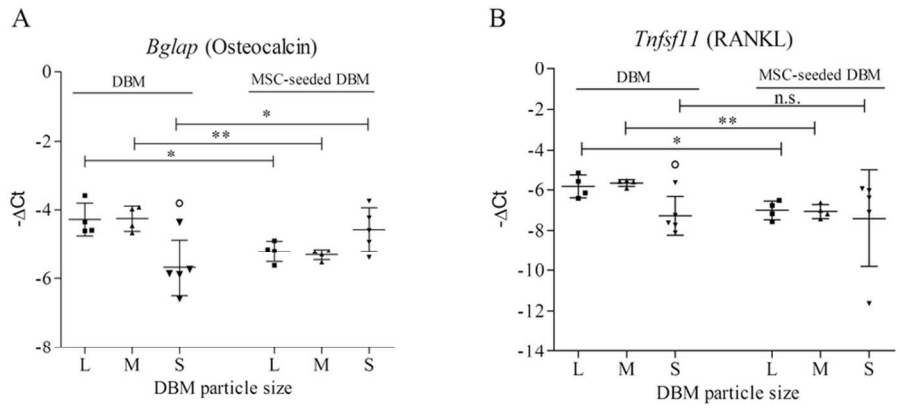

FIGURE 8. Analysis of mouse gene expression in recovered implants following 8-week subcutaneous implantation period. Bglap (Osteocalcin) (A) and Tnfsf11 (RANKL) (B) gene expression was normalized to GAPDH and results are reported as –ΔCt. Differences between three different particle sizes (L= large; M= medium, S= small) in the DBM group and the MSC-seeded DBM group are reported with °. Differences between DBM of each particle size with and without MSC are reported with *. ° $p<0.05$; * $p<0.05$; ** $p<0.01$; n.s. not significance

87x41mm (300 x 300 DPI)